Inorganic Chemistry

Article

pubs.acs.org/IC

Crystal Growth, Structures, and Properties of the Complex Borides, $LaOs_2Al_2B$ and $La_2Os_2AlB_2$

Daniel E. Bugaris,[†] Fei Han,[†] Jino Im,[‡,§] Duck Young Chung,[†] Arthur J. Freeman,[‡] and Mercouri G. Kanatzidis*[,†,∥]

[†]Materials Science Division, Argonne National Laboratory, Argonne, Illinois 60439, United States

[‡]Department of Physics and Astronomy, Northwestern University, Evanston, Illinois 60208, United States

[§]Advanced Material Division, Korea Research Institute of Chemical Technology, Daejeon 305-600, Korea

[∥]Department of Chemistry, Northwestern University, Evanston, Illinois 60208, United States

Supporting Information

ABSTRACT: Single crystals of two novel quaternary metal borides, $LaOs_2Al_2B$ and $La_2Os_2AlB_2$, have been grown from La/Ni eutectic fluxes. $LaOs_2Al_2B$ crystallizes in tetragonal space group $P4/mmm$ with the $CeCr_2Si_2C$-type structure, and lattice parameters a = 4.2075(6) Å and c = 5.634(1) Å. $La_2Os_2AlB_2$ exhibits a new crystal structure in monoclinic space group $C2/c$ with lattice parameters a = 16.629(3) Å, b = 6.048(1) Å, c = 10.393(2) Å, and β = 113.96(3)°. Both structures are three-dimensional frameworks with unusual coordination (for solid-state compounds) of the boron atoms by transition metal atoms. The boron atom is square planar in $LaOs_2Al_2B$, whereas it exhibits linear and T-shaped geometries in $La_2Os_2AlB_2$. Electrical resistivity measurements reveal poor metal behavior ($\rho_{300\ K} \sim 900\ \mu\Omega$ cm) for $La_2Os_2AlB_2$, consistent with the electronic band structure calculations, which also predict a metallic character for $LaOs_2Al_2B$.

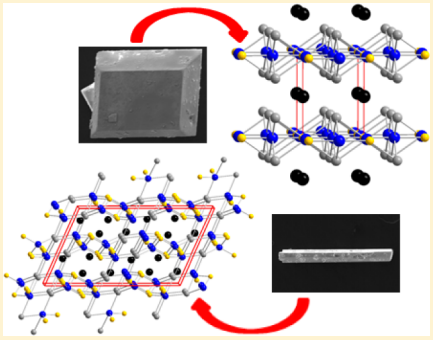

INTRODUCTION

Metal borides (and related borocarbides, boronitrides, etc.) are a highly interesting yet underexplored class of materials. Perhaps the most well-known example is MgB_2, a simple binary compound, whose existence was reported in the early 1900s and structure was determined in 1953.[1] However, it was not until 2001 that it was discovered to be superconducting, with a T_c = 39 K, highest among the conventional superconductors.[2] According to the Bardeen−Cooper−Schrieffer (BCS) theory of conventional superconductivity, high-frequency phonons are thought to play a significant role toward increasing T_c. Consequently, materials with low atomic mass elements, such as boron, have been investigated in the search for novel superconductors. Other metal borides reported to exhibit superconductivity include Li_2Pd_3B,[3] $Mg_{10}Ir_{19}B_{16}$,[4] $La_3Ru_8B_6$,[5] and $RERh_4B_4$ (RE = rare-earth element),[6] as well as borocarbides such as REM_2B_2C (M = Ni, Pd),[7] and boronitrides such as $La_3Ni_2B_2N_3$.[8]

Besides superconductivity, metal borides are known to display a variety of other interesting and useful physical properties. $Nd_2Fe_{14}B$ is one of, if not the most common, permanent magnetic materials, found in everything from commercial hard drives to electric generators and motors to magnetic resonance imaging (MRI) instruments. In the search for other metal borides that exhibit unusual magnetic behavior, materials such as $Ti_{9-x}Fe_{2+x}Ru_{18}B_8$ (x = 0, 1, 2) have been reported, where the magnetism can be tuned from ferromagnetism to ferrimagnetism by varying the Ti/Fe content.[9] Heavy fermion behavior has been discovered in $YbAlB_4$,[10] while SmB_6 is thought to be a topological Kondo insulator.[11] The metal diborides, OsB_2 and ReB_2, have been reported to be ultra-incompressible hard materials,[12] making them candidates for applications such as abrasives, cutting tools, and scratch-resistant coatings.

Despite the wide range of magnetic, electronic, and structural phenomena they exhibit, metal borides have been researched far less as compared to other classes of materials, such as oxides or chalcogenides. The main reason for this is their difficult synthesis, which can be attributed to the extremely high melting point of boron (mp = 2076 °C), making it among the most refractory elements in the periodic table. To overcome this obstacle, metal borides have traditionally been prepared by the brute force technique of arc-melting (often followed by high-temperature annealing for an extended period of time). In order to search for novel metal borides with potentially interesting properties, perhaps in "low" to intermediate temperature regimes, other techniques have been developed and are currently still being refined. Some of these techniques will be described further in the Results and Discussion section below.

Herein, we report the discovery of two novel quaternary metal borides, $LaOs_2Al_2B$ and $La_2Os_2AlB_2$. Single crystals of these two compounds were grown from a La/Ni metal eutectic

Received: June 5, 2015
Published: August 4, 2015

DOI: 10.1021/acs.inorgchem.5b01275
Inorg. Chem. 2015, 54, 8049−8057

flux, applied for the first time to the osmium−boron chemical system. The structures of both materials were determined by single-crystal X-ray diffraction. $LaOs_2Al_2B$ crystallizes in the $CeCr_2Si_2C$-type structure,[13] whereas $La_2Os_2AlB_2$ possesses a new structure type. Both crystal structures are three-dimensional frameworks with unusual linear, T-shaped, and square planar coordination of boron by osmium atoms. Electrical resistivity measurements on single crystals of $La_2Os_2AlB_2$ reveal metallic behavior. Electronic band structure calculations suggest a metallic character for both boride compounds.

EXPERIMENTAL METHODS

General Details. The following reagents were used as received: lanthanum (Alfa Aesar, 99.9%), osmium (Goldsmith Bros., 99.9%), aluminum (Alfa Aesar, 99.97%), and boron (Alfa Aesar, 98%). La/Ni eutectic (Alfa Aesar, 88:12 wt %) was received as a single ingot but was broken apart into small pieces prior to use. Handling of materials was performed in an M-Braun glovebox under an inert Ar atmosphere (<0.1 ppm of H_2O and O_2).

Crystal Growth of $LaOs_2Al_2B$. La (0.0926 g, 0.66 mmol), Os (0.2536 g, 1.32 mmol), Al (0.0260 g, 1.32 mmol), and B (0.0072 g, 0.66 mmol) were placed in a 2 mL alumina crucible. The reaction mixture was covered with 1 g of La/Ni eutectic. The alumina crucible was placed in a 15 mm o.d. × 13 mm i.d. fused-silica tube, covered by an inverted alumina crucible filled with quartz wool, and flame-sealed under a vacuum of $<10^{-4}$ mbar. In a programmable furnace, the tube was heated to 1000 °C in 3 h, held at 1000 °C for 12 h, cooled to 850 °C in 10 h, held at 850 °C for 48 h, and then cooled to 600 °C in 84 h. Upon reaching 600 °C, the quartz tube was removed from the furnace, inverted, and quickly centrifuged. Some of the La/Ni eutectic flux was removed by the centrifugation step, while the rest remained in the alumina crucible with the products. After opening the quartz tube, the product could be left in the air to oxidize the flux, resulting in La_2O_3 (hydrolyzes to $La(OH)_3$ in moist air) powder and Ni particles. Metallic black plate crystals of $LaOs_2Al_2B$ could be manually isolated.

Crystal Growth of $La_2Os_2AlB_2$. La (0.0772 g, 0.55 mmol), Os (0.2114 g, 1.10 mmol), Al (0.0300 g, 1.10 mmol), and B (0.0060 g, 0.55 mmol) were placed in a thin niobium tube that had been sealed at one end with a Centor arc welder. The reaction mixture was covered with 1.2 g of La/Ni eutectic. The niobium tube was placed in a 15 mm o.d. × 13 mm i.d. fused-silica tube, covered with a small plug of quartz wool, and flame-sealed under a vacuum of $<10^{-4}$ mbar. The same heating profile and centrifugation procedure as described above for $LaOs_2Al_2B$ were utilized here. Following oxidation of the remaining flux, metallic black columnar crystals of $La_2Os_2AlB_2$ could be manually isolated.

Scanning Electron Microscopy. The microprobe analyses of several crystals were performed with a Hitachi S-4700-II Scanning Electron Microscope using an EDAX Phoenix X-ray energy dispersive spectrometer (EDS). The spectrometer utilizes a Li-drifted Si detector with an ultrathin window, and data were acquired with a beam current of 10 μA at 20 kV accelerating potential. Semiquantitative analysis by EDS on several crystals confirmed the presence of La, Os, and Al. The boron content could not be confirmed due to the limitation of EDS with elements lighter than Na. No Ni or Nb impurities (from the flux and reaction vessel, respectively) were detected in the crystals.

Single Crystal X-ray Diffraction. Single crystals of $LaOs_2Al_2B$ and $La_2Os_2AlB_2$ were selected and mounted on the tips of glass fibers for X-ray diffraction. Intensity data were collected at 298 K using ω scans on a STOE 2T imaging plate diffraction system using graphite-monochromatized Mo Kα radiation (λ = 0.71073 Å) operating at 50 kV and 40 mA with a 34 cm diameter imaging plate. Individual frames were collected with a 5 min exposure time and a 0.5° ω rotation for $LaOs_2Al_2B$ and a 4 min exposure time and a 0.3° ω rotation for $La_2Os_2AlB_2$. X-AREA, X-RED, and X-SHAPE software packages were used for data collection, integration, and analytical absorption corrections, respectively.[14] Structures were solved with the direct methods program SHELXS and refined with the full-matrix least-squares program SHELXL.[15] Each final refinement included a secondary extinction correction. The parameters for data collection and details of the structure refinements are given in Table 1. Atomic coordinates and thermal displacement parameters (U_{eq}) are given in Table 2, and selected interatomic distances and angles are given in Tables 3 and 4.

Table 1. Structure Refinement Details from Single-Crystal X-ray Diffraction[a]

	$LaOs_2Al_2B$	$La_2Os_2AlB_2$
formula weight	584.08	706.82
crystal system	tetragonal	monoclinic
space group	*P*4/*mmm*	*C*2/*c*
a (Å)	4.2075(6)	16.629(3)
b (Å)	4.2075(6)	6.048(1)
c (Å)	5.634(1)	10.393(2)
β (deg)	90	113.96(3)
volume (Å^3)	99.74(3)	955.2(3)
Z	1	8
ρ_c (g/cm^3)	9.724	9.830
μ (mm^{-1})	74.260	70.557
F(000)	240	2312
crystal size (mm)	0.134 × 0.127 × 0.050	0.342 × 0.047 × 0.040
θ range for data collection (deg)	4.84 to 27.59	3.93 to 29.99
index ranges	$-5 \le h \le 4$	$-23 \le h \le 23$
	$-5 \le k \le 5$	$-8 \le k \le 8$
	$-7 \le l \le 6$	$-14 \le l \le 14$
reflections collected	843	4794
independent reflections	97 [R_{int} = 0.1253]	1395 [R_{int} = 0.0588]
completeness	99% to θ = 27.59°	99.6% to θ = 29.99°
refinement method	full-matrix least-squares on F^2	full-matrix least-squares on F^2
data/restraints/parameters	97/0/12	1395/0/65
GOF	1.190	1.381
final *R* indices [>2σ(I)][b]	R_{obs} = 0.0384	R_{obs} = 0.0259
	wR_{obs} = 0.0950	wR_{obs} = 0.0593
R indices [all data][b]	R_{all} = 0.0384	R_{all} = 0.0262
	wR_{all} = 0.0950	wR_{all} = 0.0594
extinction coefficient	0.22(3)	0.00140(5)

[a]For both structures, T = 298(2) K and λ = 0.71073 Å. [b]$R = \sum ||F_o| - |F_c|| / \sum |F_o|$, $wR = \{\sum [w(|F_o|^2 - |F_c|^2)^2] / \sum [w(|F_0|^4)]\}^{1/2}$ and calcd $w = 1/[\sigma^2(F_0^2) + (A \times P)^2 + (B \times P)]$ where $P = (F_o^2 + 2F_c^2)/3$. For $LaOs_2Al_2B$, A = 0.0704 and B = 0.2238. For $La_2Os_2AlB_2$, A = 0.0210 and B = 14.7714.

Electrical Resistivity. Electrical resistivity as a function of temperature was measured on a single crystal of $La_2Os_2AlB_2$ by the four-probe method using a Quantum Design Physical Property Measurement System. The four-probe geometry was implemented with 35 μm gold wires acting as the current and voltage electrodes, attached to the crystal via conductive silver paste (DuPont 4929N). The temperature range for the measurement was 1.8−300 K. Without single crystals of adequate size, the electrical resistivity of $LaOs_2Al_2B$ could not be measured.

Magnetic Susceptibility. Zero-field-cooled (ZFC) magnetic susceptibility data were collected under a low applied field of 1 G beginning at 1.8 K in a home-built SQUID to test for possible superconductivity. The measurement was performed on an impure polycrystalline sample of $La_2Os_2AlB_2$ and byproducts, as well as a few small single crystals of $LaOs_2Al_2B$. A hint of superconductivity was detected at ∼6 K, most likely due to residual β-La from the flux, as had been reported previously with La/Ni flux experiments.[16] Otherwise, no superconductivity originating from either main phase was observed.

DOI: 10.1021/acs.inorgchem.5b01275
Inorg. Chem. 2015, 54, 8049−8057

Table 2. Atomic Coordinates and Equivalent Isotropic Displacement Parameters (Å^2 × 10^3) for $LaOs_2Al_2B$ and $La_2Os_2AlB_2$

atom	Wyckoff	x	y	z	U_{eq}[a]
			$LaOs_2Al_2B$		
La	1*b*	0	0	0.5	11(1)
Os	2*f*	0	0.5	0	10(1)
Al	2*h*	0.5	0.5	0.261(1)	11(2)
B	1*a*	0	0	0	10(7)
			$La_2Os_2AlB_2$		
La(1)	8*f*	0.2464(1)	0.3342(1)	0.3496(1)	6(1)
La(2)	8*f*	0.4445(1)	0.1002(1)	0.3331(1)	7(1)
Os(1)	8*f*	0.0768(1)	0.0737(1)	0.3678(1)	6(1)
Os(2)	8*f*	0.1710(1)	0.3295(1)	0.0158(1)	5(1)
Al	8*f*	0.0726(2)	0.0978(4)	0.1014(3)	7(1)
B(1)	8*f*	0.1119(6)	0.380(1)	0.441(1)	9(2)
B(2)	8*f*	0.3079(6)	0.403(1)	0.121(1)	9(2)

[a] U_{eq} is defined as one-third of the trace of the orthogonalized U_{ij} tensor.

Table 3. Selected Interatomic Distances (Å) for $LaOs_2Al_2B$

La−B × 2	2.8169(5)
La−Al × 8	3.265(3)
La···Os × 8	3.5158(5)
Os−B × 2	2.1037(3)
Os−Al × 4	2.568(4)
Os···Os × 4	2.9752(4)
Al−Os × 4	2.568(4)
Al−Al	2.69(2)
Al···Al	2.95(2)
B−Os × 4	2.1037(3)
B−La × 2	2.8169(5)

Band Structure Calculations. The electronic structures of $LaOs_2Al_2B$ and $La_2Os_2AlB_2$ were investigated from first-principles calculations using density functional theory (DFT). The projector augmented wave (PAW) method,[17] implemented in the Vienna Ab initio Simulation Package (VASP),[18] was employed. The exchange correlation interactions were described by the generalized gradient approximation within the Perdew−Burke−Ernzerhof (PBE) formalism.[19] The cutoff energy for the plane wave basis was set to 350 eV, and 12 × 12 × 9 and 9 × 9 × 5 regular meshes were chosen for momentum space sampling for $LaOs_2Al_2B$ and $La_2Os_2AlB_2$, respectively. In order to account for the strong on-site Coulomb interaction of La f orbitals, we used the DFT+U approach with an effective Hubbard parameter, $U_{eff} = U - J = 8.0$ eV.[20] The band structures were plotted along high symmetry points.[21]

RESULTS AND DISCUSSION

Crystal Growth of Metal Borides. Metal borides have been one of the more challenging classes of inorganic solid-state materials in which to grow high-quality single crystals. One interesting approach to growing single crystals of metal borides is by chemical vapor transport. An early report details the growth of single-crystalline binary metal borides such as TiB_2, VB_2, CrB, CrB_2, and ZrB_2 from the elements using halogens (Cl, Br, I) as transport agents with "hot zone" temperatures of 1050−1100 °C and temperature gradients of 120−200 °C over the length of the sealed quartz reaction vessel.[22] Some more recent literature discusses the crystal growth of the tetraborides CrB_4 and MnB_4 using iodine as the mineralizer.[23] Although these results are intriguing, it appears that the utility of chemical vapor transport for crystal growth of metal borides is limited to fairly simple binary systems, but further research is warranted.

Another intermediate temperature route to grow single crystals of metal borides which has proven successful is that of molten metal fluxes. In this technique, a low melting metal (either transition element or main-group) is chosen such that it can dissolve boron, as well as other elements, and allow crystal growth to proceed at significantly reduced temperatures as compared to arc-melting. The advantage of metal fluxes over chemical vapor transport in the crystal growth of metal borides is that in addition to binary compounds, many ternary and

Table 4. Selected Interatomic Distances (Å) for $La_2Os_2AlB_2$

La(1)−B(1)	2.777(9)	La(2)−B(1)	2.86(1)	Al−Os(2)	2.572(2)
La(1)−B(1)	2.793(9)	La(2)−B(1)	2.871(9)	Al−Os(1)	2.635(2)
La(1)−B(2)	2.814(8)	La(2)−B(1)	2.93(1)	Al−Os(1)	2.667(3)
La(1)−B(2)	2.97(1)	La(2)−La(2)	2.998(1)	Al−Os(1)	2.745(3)
La(1)−B(2)	3.03(1)	La(2)−B(2)	3.051(9)	Al−Al	2.746(5)
La(1)···Os(2)	3.173(1)	La(2)···Al	3.124(2)		
La(1)···Os(2)	3.2331(7)	La(2)···Al	3.152(2)	B(1)−Os(1)	1.999(9)
La(1)···La(1)	3.245(1)	La(2)···Al	3.290(3)	B(1)−Os(2)	2.008(9)
La(1)···Os(1)	3.251(2)	La(2)···Os(2)	3.3594(8)	B(1)−La(1)	2.793(9)
La(1)···Al	3.258(2)	La(2)···Os(2)	3.371(1)	B(1)−La(2)	2.86(1)
La(1)···Os(1)	3.3025(7)	La(2)···La(1)	3.372(1)	B(1)−La(2)	2.871(9)
La(1)···Al	3.316(3)	La(2)···La(2)	3.422(1)	B(1)−La(2)	2.93(1)
La(1)···Os(2)	3.3545(8)	La(2)···Os(1)	3.4766(7)		
La(1)···La(2)	3.373(1)	La(2)···Os(2)	3.489(1)	B(2)−Os(2)	2.131(9)
La(1)···Os(2)	3.4061(8)	La(2)···Os(1)	3.5400(7)	B(2)−Os(2)	2.133(9)
				B(2)−Os(1)	2.139(9)
Os(1)−B(1)	1.999(9)	Os(2)−B(1)	2.008(9)	B(2)−La(1)	2.814(8)
Os(1)−B(2)	2.139(9)	Os(2)−B(2)	2.131(9)	B(2)−La(1)	3.03(1)
Os(1)−Al	2.635(2)	Os(2)−B(2)	2.133(9)		
Os(1)−Al	2.667(3)	Os(2)−Al	2.572(2)		
Os(1)−Os(1)	2.728(1)	Os(2)···Os(2)	2.9375(7)		
Os(1)−Al	2.745(3)	Os(2)···Os(1)	2.9682(7)		
Os(1)···Os(2)	2.9682(7)				

DOI: 10.1021/acs.inorgchem.5b01275
Inorg. Chem. 2015, 54, 8049−8057

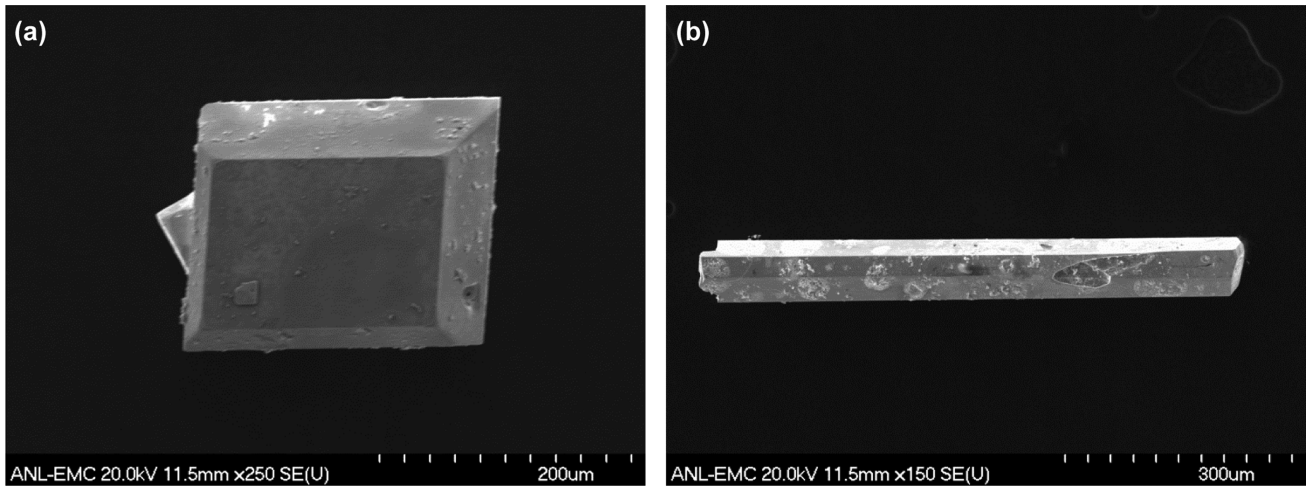

Figure 1. SEM micrographs of typical crystals of (a) $LaOs_2Al_2B$ and (b) $La_2Os_2AlB_2$. Some residue from the La/Ni flux is visible on the surfaces.

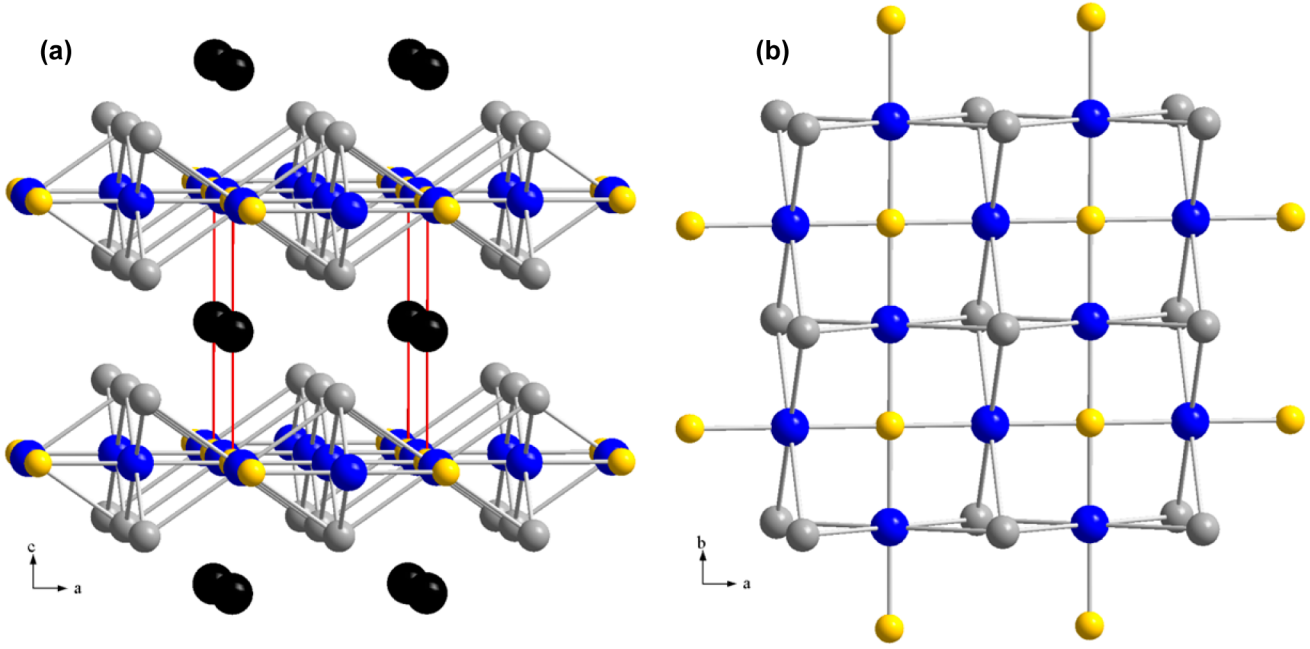

Figure 2. (a) Crystal structure of $LaOs_2Al_2B$ as viewed along the *b* axis. La, Os, Al, and B atoms are shown as black, blue, gray, and gold spheres, respectively. (b) Two-dimensional $[Os_2Al_2B]$ layer as viewed along the *c* axis. The unusual square planar coordination of B by four Os atoms is evident.

higher order materials have also been prepared. Among the metals that have been tried, the most effective, at least based on the number of references in the literature, seem to be aluminum and copper. A representative listing of materials grown as single crystals from aluminum flux includes $AAlB_{14}$ (A = Li, Na, Mg, Y, Er, Tm),[24] $REAlB_4$ (RE = Ho–Lu),[25] RE_2AlB_6 (RE = Sc, Lu),[25b,26] and $Ni_{20+x}Al_{3-x-2y}B_{6+8y}$.[27] Although Al can be used as an "inert" metal flux for the growth of binary metal borides, in more complex systems it instead serves as a reactive flux and is incorporated into the ternary metal boride products. Copper, on the other hand, acts solely as an inert metal flux for the dissolution of boron; some complex metal borides crystallized from copper include $RERh_3B$ (RE = Sm, Gd, Er, Tm),[28] $RERh_3B_2$ (RE = Gd, Dy, Er–Lu),[28] $RERh_4B_4$ (RE = Sm, Gd–Tm),[29] and $PrRh_{4.8}B_2$.[30] Besides Al and Cu, other molten metal fluxes used for the crystal growth of borides are the following: Li ($Li_2Rh_3B_2$,[31] $Sr_2Ru_7B_8$[32]), Na ($NaPt_3B_{1+x}$[33]), Co ($MoCoB$[34]), Zn ($ZnIr_2B_2$[35]), Ga ($Ni_{12}GaB_8$ and $Ni_{10.6}Ga_{0.4}B_6$[36]), and Sn ($Er_8Si_{17}B_3$[37]).

Building on the earlier success of these molten metal fluxes, more complex elemental mixtures have been explored for the crystal growth of metal borides. The first example of this was the pioneering work by Canfield et al. using the Ni_2B binary compound in the crystal growth of the quaternary $RENiB_2C_2$ superconductors.[38] Ni and B in a 2:1 ratio form a "low-melting" eutectic mixture at 1125 °C, which acts as a molten flux to grow large, high-quality single crystals of $RENiB_2C_2$ phases. Although Cava et al. were the first to report on superconductivity[7a] in this system (on samples that had been arc-melted), it was the availability of large single crystals from Ni_2B flux that allowed the solid-state chemistry and condensed matter physics communities to thoroughly investigate the structural and physical properties of these interesting materials.

DOI: 10.1021/acs.inorgchem.5b01275
Inorg. Chem. 2015, 54, 8049–8057

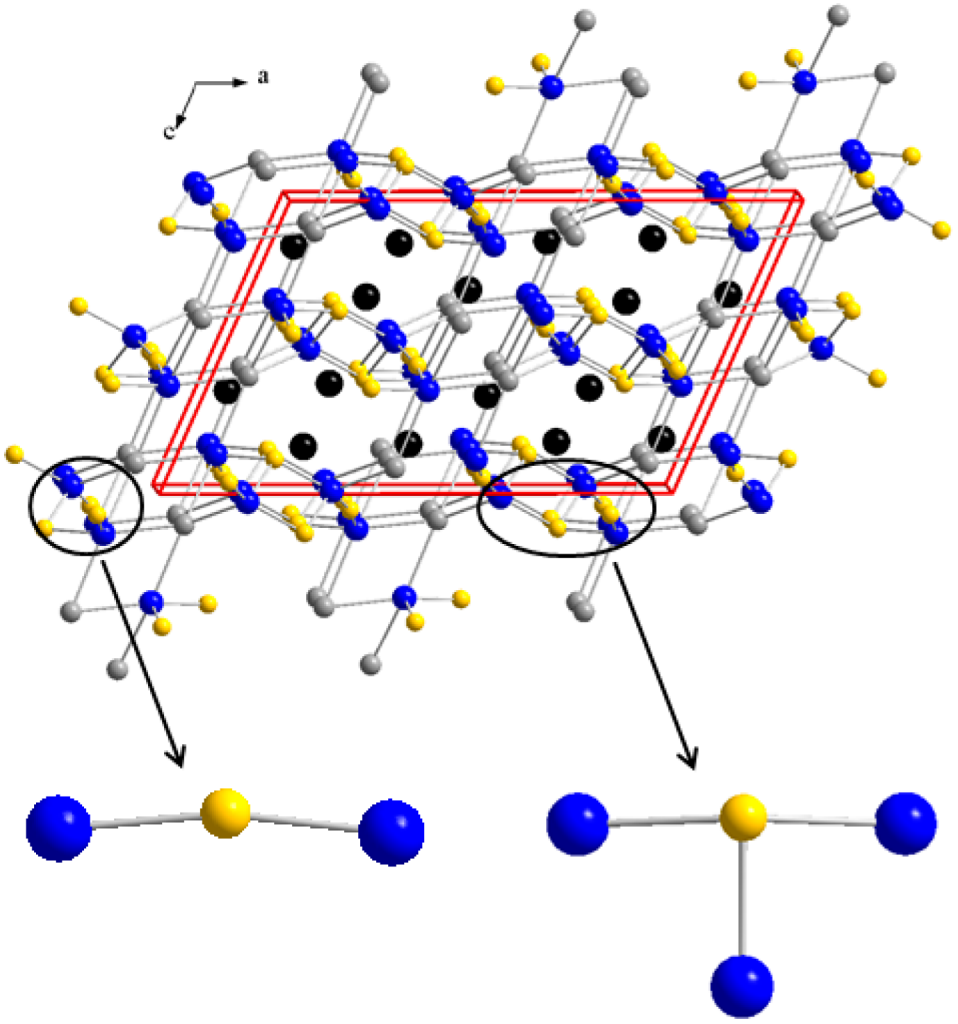

Figure 3. Crystal structure of $La_2Os_2AlB_2$ as viewed along the *b* axis. La, Os, Al, and B atoms are shown as black, blue, gray, and gold spheres, respectively. Highlighted are the rare linear and T-shaped coordination geometries of B(1) and B(2), respectively.

More recently, Latturner et al. have developed a series of low-melting metal eutectic mixtures that are composed of a rare-earth element and a transition metal. For example, an 88:12 ratio of La to Ni melts at 532 °C, much lower than the melting points of either individual element (918 and 1455 °C, respectively). Not only do these metal eutectics have conveniently low melting points, but they have also proven to be effective at dissolving large quantities of main group elements. As such, it has been possible to grow single crystals of many novel phases, including borides and borocarbides such as $LaRu_2Al_2B$,[16] $RE_{33}Fe_{14-x}Al_{x+y}B_{25-y}C_{34}$ (RE = La, Ce), and $RE_{33}Fe_{13-x}Al_xB_{18}C_{34}$ (RE = Ce, Pr).[39]

In the present work, we set out to explore the reactivity of the 5d transition metal Os with B in the La/Ni eutectic metal flux. Similar to boron, Os is highly refractory, with the third-highest melting point among transition metals. For this reason, the vast majority of Os borides have been prepared by arc-melting, most often yielding polycrystalline products. Furthermore, the compounds that have been reported in the literature have primarily been limited to binary and ternary Os borides. Although some pseudoternary phases such as $La(Os_{4-x}Ir_x)B_4$ (x = 1, 2, 3)[40] have been reported, the only true (pseudo)quaternary Os borides, to the best of our knowledge, are $Ti_{1.6}Os_{1.4}RuB_2$,[41] $(Ti_{0.75}Fe_{0.25})Os_2RhB_2$, and $(Ti_{0.67}Fe_{0.33})Os_2RhB_2$.[42]

We have successfully grown metallic black single crystals (Figure 1) of the new quaternary borides, $LaOs_2Al_2B$ and $La_2Os_2AlB_2$. Both phases were synthesized starting from the same 1:2:2:1 ratio of elements mixed with La/Ni eutectic flux. A higher flux:reagent ratio was used in the preparation of $La_2Os_2AlB_2$, which may explain the higher concentration of La in the final product. Another difference is that $LaOs_2Al_2B$ was synthesized using an alumina crucible as the reaction vessel, whereas $La_2Os_2AlB_2$ was grown in a niobium tube. The La/Ni flux is known to aggressively etch alumina crucibles at high temperatures, possibly leaching excess aluminum into the solute/solvent mixture, which yields the more Al-rich $LaOs_2Al_2B$.

Crystal Structure of $LaOs_2Al_2B$. $LaOs_2Al_2B$ crystallizes in tetragonal space group *P*4/*mmm* with the three-dimensional $CeCr_2Si_2C$ structure type[13] (Figure 2a). The unit cell parameters are $a = b = 4.2075(6)$ Å and $c = 5.634(1)$ Å. There is one crystallographic site for each atom type. All atoms are located on special positions, with site symmetries of 4/*mmm* for La and B, *mmm* for Os, and 4*mm* for Al (Table 2).

$LaOs_2Al_2B$ is composed of $[Os_2Al_2B]$ layers (Figure 2b) that are separated by La atoms. The layers consist of a square net of

DOI: 10.1021/acs.inorgchem.5b01275
Inorg. Chem. 2015, 54, 8049−8057

Os atoms; alternating squares are centered by B atoms. This creates a planar [Os_2B] sheet with a checkerboard pattern. Each Os atom is bonded to two B atoms at distances of 2.1037(3) Å. These are typical of Os−B bond lengths, which are observed to be 2.0846(7)−2.220(1) Å in $LaOs_2B_2$.[43] The Al atoms are located above and below the [Os_2B] sheet such that each Os atom is coordinated by a square planar arrangement of four Al atoms at a bonding distance of 2.568(4) Å. This Os−Al bond length is comparable to those observed in $Y_{7.86(1)}Os_{12}Al_{61.51(4)}$, which range from 2.562 to 2.680 Å.[44] With four equatorial Al atoms and two axial B atoms, the Os atom exhibits an octahedral coordination geometry. At an interatomic distance of 2.9752(4) Å, there may also be weak metal−metal interactions between adjacent Os atoms within the planar square net.

Each Al atom is bonded to four Os atoms in the square net above or below it. Additionally, there is an interlayer Al−Al bond distance of 2.69(2) Å. These bonds connect adjacent [Os_2Al_2B] layers in order to form a three-dimensional framework. There are also weak Al···Al interactions at 2.95(2) Å within the [Os_2Al_2B] layers. Each B atom located in the [Os_2Al_2B] layers is bonded to four Os atoms in a highly unusual square planar arrangement. When bonded to transition metals, B is most commonly found to a have a trigonal prismatic or octahedral coordination by six transition metal atoms,[45] or a square antiprismatic coordination by eight transition metal atoms.[46] The only other solid-state compounds to exhibit a square planar geometry around a central boron atom are the isostructural compounds $RERu_2M_2B$ (RE = La, Ce, Pr, Nd, Sm; M = Al, Ga),[16,47] as well as the ternary compounds Ga_8Ir_4B[48] and $Y_2Pd_{14}B_5$.[49] Boron with a square planar coordination by transition metals is equally rare in molecular chemistry, with the only known examples being [{(η^5-C_5Me_5)$Fe(CO)_2$}{$Cr(CO)_5$}{$Pt(PCy)$}$_2${η^4-B}] and [{η^5-C_5H_5)$Mn(CO)_2$}$_2${$Pt(PCy)$}{(ITol)Au}{η^4-B}].[50]

The La atom is coordinated by 18 atoms (two B, eight Al, and eight Os) in a cage-like arrangement. The B atoms are located directly above and below the La atom, with a La−B bond distance of 2.8169(5) Å, which is similar to the range of La−B distances (2.884(3)−3.0999(7) Å) found in $LaOs_2B_2$.[43] The eight La···Al interactions at 3.265(3) Å are comparable to those in LaAl which range from 3.2316(6) to 3.5925(3) Å.[51] The interatomic distance for La···Os is 3.5158(5) Å, as compared to 3.048(2)−3.717(1) Å observed in $LaOs_2B_2$.

Crystal Structure of $La_2Os_2AlB_2$. $La_2Os_2AlB_2$ crystallizes in monoclinic space group $C2/c$ with a novel three-dimensional framework structure (Figure 3). The unit cell parameters are a = 16.629(3) Å, b = 6.048(1) Å, c = 10.393(2) Å, and β = 113.96(3)°. There are two crystallographic sites each for La, Os, and B, but only one for Al. All of the atoms are located on general positions (Table 2).

$La_2Os_2AlB_2$ contains an [Os_2AlB_2] network with La atoms occupying the voids. Os(1) exhibits an approximately square pyramidal geometry, with coordination by two B atoms and three Al atoms. The apical Os(1)−B(1) bond length is 1.999(9) Å, while the basal Os(1)−B(2) length is 2.139(9) Å. The three basal Os(1)−Al bond distances are 2.635(2) Å, 2.667(3) Å, and 2.745(3) Å. Os(2) is tetrahedrally coordinated by three B atoms and one Al atom. Os(2) is bonded with one B(1) atom and two B(2) atoms at distances of 2.008(9) Å, 2.131(9) Å, and 2.133(9) Å, respectively. The Os(2)−Al bond length is 2.572(2) Å. Both the Os(1) square pyramid and the Os(2) tetrahedron are highly distorted due to the ∼0.5 Å difference between the Os−B and Os−Al bond lengths. The short Os−B bond distances of 1.999(9) Å and 2.008(9) Å are atypical, yet even shorter Os−B bond lengths of 1.948(2) Å and 1.974(1) Å are observed in $Ca_2Os_3B_5$ and $Eu_2Os_3B_5$, respectively.[52] The remaining Os−B and Os−Al bond distances in $La_2Os_2AlB_2$ are comparable to those observed in $LaOs_2B_2$ and $Y_{7.86(1)}Os_{12}Al_{61.51(4)}$, as given above.

The Os(1) square pyramids form twisting helices along the c axis. Each Os(1)B_2Al_3 unit shares two edges and two corners with adjacent units. The edge-sharing results in short metal−metal bonds between Os(1) atoms with a length of 2.728(1) Å. Each Os(2)B_3Al tetrahedron shares an edge with a neighboring tetrahedron to form a dimeric unit, with a weak metal−metal interaction between Os(2) atoms at a distance of 2.9375(7) Å. These Os(2) dimers are directed along the a axis and serve to stitch the Os(1) helices together in order to form the three-dimensional [Os_2AlB_2] framework (Figure 4). At an interatomic distance of 2.9682(7) Å, there may also be weak metal−metal interactions between Os(1) and Os(2) atoms.

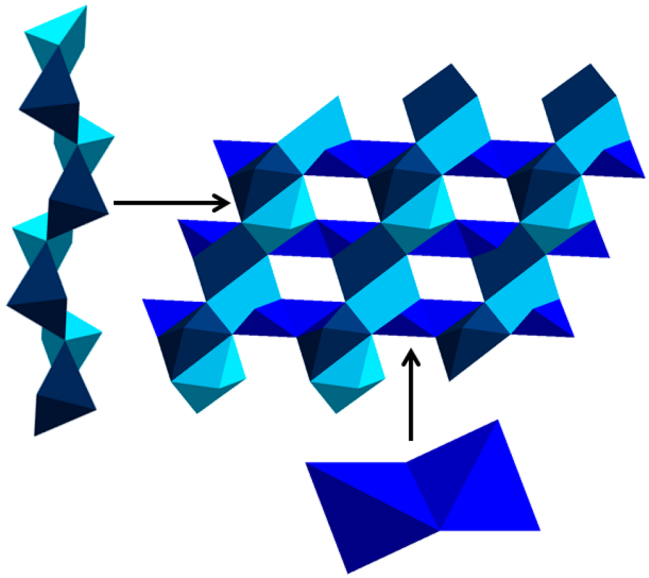

Figure 4. Polyhedral representation of $La_2Os_2AlB_2$. Os(1) square pyramids, shown in dark blue and light blue, edge- and corner-share to form twisting helices. Os(2) tetrahedra, shown in blue, share edges to create dimeric units.

Each Al atom is five-coordinate, with bonds to four Os atoms as well as one Al atom. The Al−Al bond length is 2.746(5) Å. Both B atoms possess unique coordination geometries, with only two and three B−Os bonds, respectively (Figure 3). The [Os(1)−B(1)−Os(2)] unit is nearly linear, with a bond angle of 168.4(5)°. B(2) has a distorted T-shaped coordination, with three approximately equal B(2)−Os bond distances. Two of the Os−B(2)−Os bond angles are slightly less than 90° (87.1(3)° and 88.1(4)°), while the third Os−B(2)−Os bond angle is 151.0(5)°, which is significantly less than the 180° bond angle found in regular T-shaped coordination. To the best of our knowledge, these are the only examples of B atoms in a solid-state compound that are coordinated by only two or three transition metal atoms. A linear bonding environment with two transition metals is nearly as rare in molecular chemistry, with the only two reported examples being [{(η^5-C_5Me_5)$Fe(CO)_2$}{$Fe(CO)_4$}{η^2-B}] and [{(η^5-C_5Me_5)Fe-$(CO)_2$}{$Cr(CO)_5$}{η^2-B}].[53] The T-shaped coordination by

DOI: 10.1021/acs.inorgchem.5b01275
Inorg. Chem. 2015, 54, 8049−8057

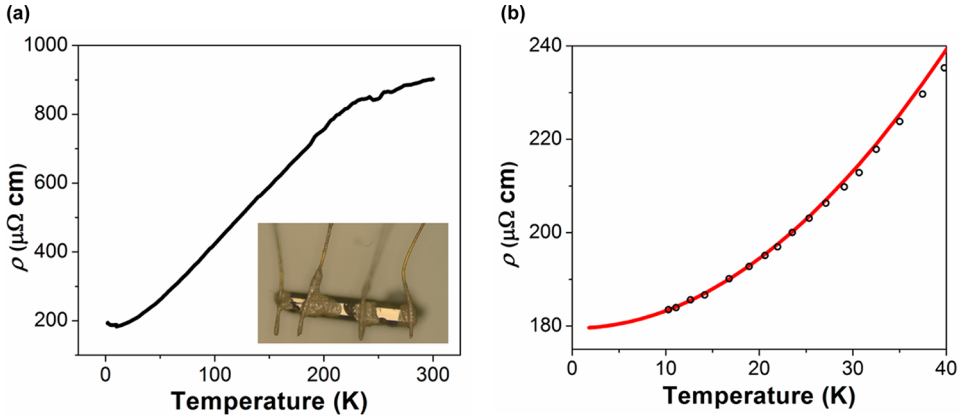

Figure 5. (a) Temperature-dependent electrical resistivity of $La_2Os_2AlB_2$ in the temperature range 1.8−300 K. The inset shows a typical single crystal of $La_2Os_2AlB_2$ used for the measurement. (b) Fitting (red line) of $\rho(T) = \rho_0 + AT^n$ to the low-temperature data (black circles), yielding values of ρ_0 = 179.5(5) $\mu\Omega$ cm and n = 1.99(9).

three transition metals, on the other hand, is more common among molecular complexes.[50,54]

La(1) and La(2) are each coordinated by 15 atoms. The La−B bond distances are in the range 2.777(9)−3.051(9) Å, which are similar to those found in $LaOs_2B_2$, as mentioned above. There is one short metal−metal bond between La(2) atoms with a length of 2.998(1) Å. Although this is less than the sum of La metallic radii (3.38 Å), such a short La−La bond distance is not without precedent. For example, La_4LiAuO_8[55] and $(Ca_{0.906}La_{0.094})La_6OsI_{12}$[56] exhibit La−La metal bonds with lengths of 2.5127 Å and 2.865(1) Å, respectively. All other La···La, La···Al, and La···Os interactions are normal.

Electrical Resistivity of $La_2Os_2AlB_2$. The electrical resistivity of $La_2Os_2AlB_2$, as measured upon a single crystal, is shown in Figure 5a. The resistivity increases with temperature, indicative of metallic behavior. The value of the room-temperature resistivity, ρ_{300K}, is approximately 900 $\mu\Omega$ cm, which characterizes $La_2Os_2AlB_2$ as a poor metal. For comparison, the room-temperature resistivity values exhibited by some other chemically similar complex metal borides include 250 $\mu\Omega$ cm for $LaPt_2B$,[57] 950 $\mu\Omega$ cm for $Ce_3Ni_{25.75}Ru_{3.16}Al_{4.1}B_{10}$,[58] 1100 $\mu\Omega$ cm for $MgOs_3B_4$,[59] and 1700 $\mu\Omega$ cm for $Sc_2SiIr_5B_2$.[60] The small residual resistivity ratio RRR = $\rho_{300K}/\rho_{1.8K}$ = 4.5 is consistent with a large amount of disorder scattering, which may be due to the highly complex unit cell. We have fitted the $\rho(T)$ vs T curve with the function $\rho(T) = \rho_0 + AT^n$, where $\rho(T)$ is the resistivity at a given temperature, ρ_0 is the residual resistivity, and A and n are fitting parameters (Figure 5b). According to Fermi liquid theory, at low temperatures, n = 2, and electron−electron scattering is dominant over electron−phonon scattering. From the fitting to our data over the temperature range 10−25 K, values of ρ_0 = 179.5(5) $\mu\Omega$ cm and n = 1.99(9) are obtained. This indicates a Fermi liquid ground state in $La_2Os_2AlB_2$ at low temperatures.

Electronic Band Structures. The electronic structures of both $LaOs_2Al_2B$ and $La_2Os_2AlB_2$ were calculated from first principles. The band structure of $LaOs_2Al_2B$ (Figure 6a) shows that the Fermi level cuts both the valence and the conduction bands, suggesting that $LaOs_2Al_2B$ is a metal. The partial densities of states (PDOS) in Figure 6b further reveal that low energy electronic structures near the Fermi level mostly consist of Os d orbitals. Electronic states at the Fermi level are investigated with local densities of states (LDOS). As depicted in Figure 6c, the nature of electronic states at the Fermi level is

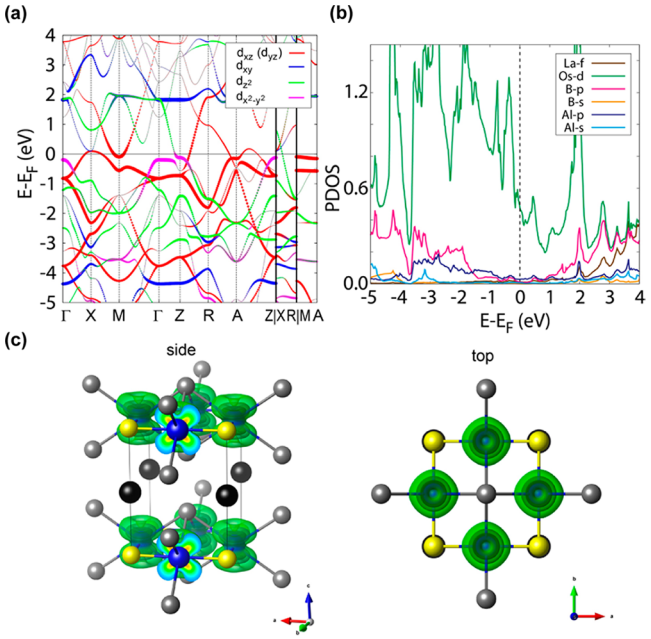

Figure 6. (a) Electronic band structure of $LaOs_2Al_2B$ with the various Os d orbitals specified. (b) Projected partial densities of states (PDOS) for the various orbital types of $LaOs_2Al_2B$. (c) A plot of the iso-surfaces with local density of states integrated in the energy range of ±0.1 eV of the Fermi level (E_F).

mostly governed by Os d_{xz} and d_{yz} orbitals which are distributed along the square lattice of Os and B. Due to the tetragonal symmetry of the crystal structure of $LaOs_2Al_2B$, there is rotational symmetry within the *ab* plane. However, the electronic states are tightly confined within the $[Os_2Al_2B]$ layers owing to its pseudo-2D structure. This asymmetric character is also consistent with the projected band structure in Figure 6a. Bands projected to Os d_{xz} and Os d_{yz} orbitals have a highly dispersive character in the Γ−X−M plane and the Z−R−A plane, but there are flat bands along Γ to Z and M to A. This result indicates that $LaOs_2Al_2B$ may have anisotropic transport properties.

In the case of $La_2Os_2AlB_2$, the electronic band structure is more complicated due to the lower symmetry (monoclinic) of the crystal structure. However, there are some common features of the electronic band structures; $La_2Os_2AlB_2$ is also

DOI: 10.1021/acs.inorgchem.5b01275
Inorg. Chem. 2015, 54, 8049−8057

a metal with low energy electronic states mostly originating from Os d orbitals (Figures 7a and b). The metallic character of

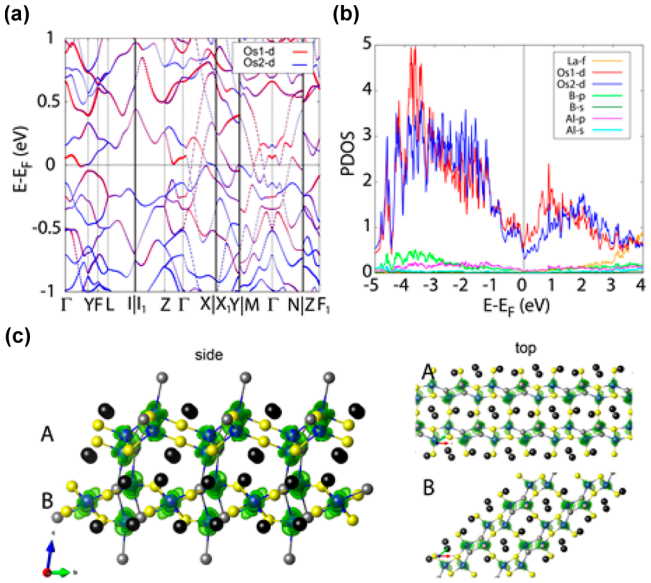

Figure 7. (a) Electronic band structure of $La_2Os_2AlB_2$ with the Os(1) and Os(2) d orbitals specified. (b) Projected partial densities of states (PDOS) for the various orbital types of $La_2Os_2AlB_2$. (c) A plot of the iso-surfaces with local density of states integrated in the energy range of ±0.1 eV of the Fermi level.

$La_2Os_2AlB_2$ is consistent with the experimental observations from the charge transport measurements. A pseudogap at the Fermi level is visible in the DOS of $La_2Os_2AlB_2$. From electronic band structure calculations, several other metal borides have been shown to exhibit pseudogaps as well. Examples of these materials include CrB_4,[23a] $M_3Ru_5B_2$ (M = Nb, Ta),[61] $Ti_{3-x}Ru_{5-y}Ir_yB_{2+x}$,[46] and Sc_2M_6B (M = Ni, Pd, Ir).[62]

The single-crystal X-ray structure refinement of $La_2Os_2AlB_2$ revealed two coordination geometries for Os, one with square pyramidal coordination (Os(1)) and the other with tetrahedral (Os(2)). PDOS in Figure 7b shows that the d orbitals of Os(1) contribute more to the electronic states at the Fermi level. LDOS analysis in Figure 7c reveals that the electronic states at the Fermi level consist of Os d orbitals which are distributed along the Os(2) dimers along the *a* axis. Along the *c* axis, a planar structure emerges via AB stacking with different orientations. The quasi-1D electronic states at the Fermi level are loosely connected via Os(1) atoms along the *c* axis and are alternatingly oriented to the *a* and *b* axes. The band structure in Figure 7a shows highly dispersive bands along Γ to X, Γ to N, and Γ to M, consistent with the quasi-1D character of the electronic states at the Fermi level.

CONCLUSION

We have extended the utility of the La/Ni eutectic metal flux for the crystal growth of Os-containing borides, namely $LaOs_2Al_2B$ and $La_2Os_2AlB_2$. Both of these compounds crystallize with three-dimensional framework structures, unique because of the bonding environments of the boron atoms. In solid-state materials, boron is most commonly found within a trigonal prismatic coordination by transition metal atoms. However, in these compounds we have discovered linear, T-shaped, and square planar geometries for the boron atoms. Besides the interesting structural features of these compounds, electronic band structure calculations predict both materials to be metallic. Electrical resistivity measurements on $La_2Os_2AlB_2$ support this hypothesis, with temperature dependence of the resistivity characteristic of a poor metal.

The recently discovered compounds $CeRu_2Al_2B$, $PrRu_2Al_2B$, and $CeRu_2Ga_2B$, which are isostructural with our $LaOs_2Al_2B$ compound, have been reported to exhibit exciting magnetic phenomena. $CeRu_2Al_2B$ is a Kondo-like system with low-temperature antiferromagnetic and ferromagnetic transitions; in the high temperature paramagnetic regime, it displays strong Ising-type magnetic anisotropy.[63] $PrRu_2Al_2B$ similarly undergoes consecutive antiferromagnetic and ferromagnetic orderings,[64] and $CeRu_2Ga_2B$ exhibits 4f localized ferromagnetism.[47] In the future, it would be of interest to replace the nonmagnetic La atom in our compounds with other rare-earth elements such as Ce or Pr to observe the magnetic behaviors that arise.

ASSOCIATED CONTENT

Supporting Information

The Supporting Information is available free of charge on the ACS Publications website at DOI: 10.1021/acs.inorgchem.5b01275.

Crystallographic data in CIF format (CIF)

AUTHOR INFORMATION

Corresponding Author

*Tel.: 847-467-1541. Fax: 847-491-5937. E-mail: m-kanatzidis@northwestern.edu.

Notes

The authors declare no competing financial interest.

ACKNOWLEDGMENTS

This work was supported as part of the Center for Emergent Superconductivity, an Energy Frontier Research Center funded by the U.S. Department of Energy, Office of Science, Office of Basic Energy Sciences. The electron microscopy was accomplished at the Electron Microscopy Center at Argonne National Laboratory, a U.S. Department of Energy Office of Science Laboratory operated under Contract No. DE-AC02-06CH11357 by UChicago Argonne, LLC.

REFERENCES

(1) Jones, M. E.; Marsh, R. E. *J. Am. Chem. Soc.* **1954**, *76*, 1434–1436.
(2) Nagamatsu, J.; Nakagawa, N.; Muranaka, T.; Zenitani, Y.; Akimitsu, J. *Nature* **2001**, *410*, 63–64.
(3) Togano, K.; Badica, P.; Nakamori, Y.; Orimo, S.; Takeya, H.; Hirata, K. *Phys. Rev. Lett.* **2004**, *93*, 247004.
(4) Klimczuk, T.; Xu, Q.; Morosan, E.; Thompson, J.; Zandbergen, H.; Cava, R. *Phys. Rev. B: Condens. Matter Mater. Phys.* **2006**, *74*, 220502.
(5) Lei, H.; Hosono, H. *Europhys. Lett.* **2013**, *104*, 17003.
(6) Matthias, B. T.; Corenzwit, E.; Vandenberg, J.; Barz, H. *Proc. Natl. Acad. Sci. U. S. A.* **1977**, *74*, 1334–1335.
(7) (a) Cava, R.; Takagi, H.; Zandbergen, H.; Krajewski, J.; Peck, W., Jr.; Siegrist, T.; Batlogg, B.; van Dover, R.; Felder, R.; Mizuhashi, K.; Lee, J.; Eisaki, H.; Uchida, S. *Nature* **1994**, *367*, 252–253. (b) Cava, R.; Takagi, H.; Batlogg, B.; Zandbergen, H.; Krajewski, J.; Peck, W., Jr.; van Dover, R.; Felder, R.; Siegrist, T.; Mizuhashi, K.; Lee, J.; Eisaki, H.; Carter, S.; Uchida, S. *Nature* **1994**, *367*, 146–148.
(8) Cava, R.; Zandbergen, H.; Batlogg, B.; Eisaki, H.; Takagi, H.; Krajewski, J.; Peck, W., Jr.; Gyorgy, E.; Uchida, S. *Nature* **1994**, *372*, 245–247.

DOI: 10.1021/acs.inorgchem.5b01275
Inorg. Chem. 2015, 54, 8049–8057

(9) (a) Fokwa, B. P.; Samolyuk, G. D.; Miller, G. J.; Dronskowski, R. *Inorg. Chem.* **2008**, *47*, 2113−2120. (b) Goerens, C.; Brgoch, J.; Miller, G. J.; Fokwa, B. P. *Inorg. Chem.* **2011**, *50*, 6289−6296.
(10) Macaluso, R. T.; Nakatsuji, S.; Kuga, K.; Thomas, E. L.; Machida, Y.; Maeno, Y.; Fisk, Z.; Chan, J. Y. *Chem. Mater.* **2007**, *19*, 1918−1922.
(11) (a) Neupane, M.; Alidoust, N.; Xu, S.-Y.; Kondo, T.; Ishida, Y.; Kim, D.; Liu, C.; Belopolski, I.; Jo, Y.; Chang, T.-R.; Jeng, H.-T.; Durakiewicz, T.; Balicas, L.; Lin, H.; Bansil, A.; Shin, S.; Fisk, Z.; Hasan, M. *Nat. Commun.* **2013**, *4*, 2991. (b) Kim, D.; Xia, J.; Fisk, Z. *Nat. Mater.* **2014**, *13*, 466−470. (c) Li, G.; Xiang, Z.; Yu, F.; Asaba, T.; Lawson, B.; Cai, P.; Tinsman, C.; Berkley, A.; Wolgast, S.; Eo, Y.; Kim, D.-J.; Kurdak, C.; Allen, J.; Sun, K.; Chen, X.; Wang, Y.; Fisk, Z.; Li, L. *Science* **2014**, *346*, 1208−1212.
(12) (a) Cumberland, R. W.; Weinberger, M. B.; Gilman, J. J.; Clark, S. M.; Tolbert, S. H.; Kaner, R. B. *J. Am. Chem. Soc.* **2005**, *127*, 7264−7265. (b) Chung, H.-Y.; Weinberger, M. B.; Levine, J. B.; Kavner, A.; Yang, J.-M.; Tolbert, S. H.; Kaner, R. B. *Science* **2007**, *316*, 436−439.
(13) Tang, C.; Fan, S.; Zhu, M. *J. Alloys Compd.* **2000**, *299*, 1−4.
(14) *X-AREA*; *X-SHAPE*; *X-RED*; STOE & Cie GMbH: Darmstadt, Germany, 2009.
(15) Sheldrick, G. *Acta Crystallogr., Sect. A: Found. Crystallogr.* **2008**, *64*, 112−122.
(16) Zaikina, J. V.; Jo, Y.-J.; Latturner, S. E. *Inorg. Chem.* **2010**, *49*, 2773−2781.
(17) Blöchl, P. E. *Phys. Rev. B: Condens. Matter Mater. Phys.* **1994**, *50*, 17953−17979.
(18) Kresse, G.; Furthmüller, J. *Phys. Rev. B: Condens. Matter Mater. Phys.* **1996**, *54*, 11169−11186.
(19) Perdew, J. P.; Burke, K.; Ernzerhof, M. *Phys. Rev. Lett.* **1996**, *77*, 3865−3868.
(20) Liechtenstein, A. I.; Anisimov, V. I.; Zaanen, J. *Phys. Rev. B: Condens. Matter Mater. Phys.* **1995**, *52*, R5467−R5470.
(21) Setyawan, W.; Curtarolo, S. *Comput. Mater. Sci.* **2010**, *49*, 299−312.
(22) Nickl, J.; Duck, M.; Pieritz, J. *Angew. Chem., Int. Ed. Engl.* **1966**, *5*, 839−840.
(23) (a) Knappschneider, A.; Litterscheid, C.; Kurzman, J.; Seshadri, R.; Albert, B. *Inorg. Chem.* **2011**, *50*, 10540−10542. (b) Knappschneider, A.; Litterscheid, C.; George, N. C.; Brgoch, J.; Wagner, N.; Beck, J.; Kurzman, J. A.; Seshadri, R.; Albert, B. *Angew. Chem., Int. Ed.* **2014**, *53*, 1684−1688.
(24) (a) Higashi, I. *J. Less-Common Met.* **1981**, *82*, 317−323. (b) Okada, S.; Tanaka, T.; Sato, A.; Shishido, T.; Kudou, K.; Nakajima, K.; Lundström, T. *J. Alloys Compd.* **2005**, *395*, 231−235. (c) Higashi, I.; Ito, T. *J. Less-Common Met.* **1983**, *92*, 239−246. (d) Korsukova, M.; Lundström, T.; Tergenius, L.-E.; Gurin, V. *J. Alloys Compd.* **1992**, *187*, 39−48. (e) Korsukova, M.; Gurin, V.; Yu, Y.; Tergenius, L.-E.; Lundström, T. *J. Alloys Compd.* **1993**, *190*, 185−187.
(25) (a) Mori, T.; Kudou, K.; Shishido, T.; Okada, S. *J. Appl. Phys.* **2011**, *109*, 07E111. (b) Okada, S.; Shishido, T.; Mori, T.; Kudou, K.; Iizumi, K.; Lundström, T.; Nakajima, K. *J. Alloys Compd.* **2006**, *408*−*412*, 547−550.
(26) Okada, S.; Tanaka, T.; Leithe-Jasper, A.; Michiue, Y.; Gurin, V. N. *J. Solid State Chem.* **2000**, *154*, 49−53.
(27) Hillebrecht, H.; Ade, M. *Angew. Chem., Int. Ed.* **1998**, *37*, 935−938.
(28) Shishido, T.; Ye, J.; Sasaki, T.; Note, R.; Obara, K.; Takahashi, T.; Matsumoto, T.; Fukuda, T. *J. Solid State Chem.* **1997**, *133*, 82−87.
(29) Zhou, H.; Chen, J.; Lambert, S.; Maple, M. *J. Appl. Phys.* **1985**, *57*, 3115−3117.
(30) Higashi, I.; Shishido, T.; Takei, H.; Kobayashi, T. *J. Less-Common Met.* **1988**, *139*, 211−220.
(31) Bailey, M. S.; Lobkovsky, E. B.; Hinks, D. G.; Claus, H.; Hor, Y. S.; Schlueter, J. A.; Mitchell, J. F. *J. Solid State Chem.* **2007**, *180*, 1333−1339.
(32) Jung, W.; Diessenbacher, F. *Z. Anorg. Allg. Chem.* **1991**, *594*, 57−65.
(33) Mirgel, R.; Jung, W. *J. Less-Common Met.* **1988**, *144*, 87−99.
(34) Jeitschko, W. *Acta Crystallogr., Sect. B: Struct. Crystallogr. Cryst. Chem.* **1968**, *24*, 930−934.
(35) Petry, K.; Jung, W. *J. Alloys Compd.* **1992**, *183*, 363−376.
(36) Ade, M.; Kotzott, D.; Hillebrecht, H. *J. Solid State Chem.* **2010**, *183*, 1790−1797.
(37) Jardin, R.; Babizhetskyy, V.; Guérin, R.; Bauer, J. *J. Alloys Compd.* **2003**, *353*, 233−239.
(38) Xu, M.; Canfield, P.; Ostenson, J.; Finnemore, D.; Cho, B.; Wang, Z.; Johnston, D. *Phys. C* **1994**, *227*, 321−326.
(39) Tucker, P. C.; Nyffeler, J.; Chen, B.; Ozarowski, A.; Stillwell, R.; Latturner, S. E. *J. Am. Chem. Soc.* **2012**, *134*, 12138−12148.
(40) Hiebl, K.; Sienko, M.; Rogl, P. *J. Less-Common Met.* **1981**, *82*, 21−28.
(41) Fokwa, B. P.; von Appen, J.; Dronskowski, R. *Chem. Commun.* **2006**, *2006*, 4419−4421.
(42) Fokwa, B. P.; Dronskowski, R. *Z. Anorg. Allg. Chem.* **2008**, *634*, 1955−1960.
(43) Horvath, C.; Rogl, P.; Hiebl, K. *J. Solid State Chem.* **1987**, *67*, 70−77.
(44) Niermann, J.; Jeitschko, W. *Inorg. Chem.* **2004**, *43*, 3264−3270.
(45) Fokwa, B. P. *Eur. J. Inorg. Chem.* **2010**, *2010*, 3075−3092.
(46) Fokwa, B. P.; Hermus, M. *Inorg. Chem.* **2011**, *50*, 3332−3341.
(47) Baumbach, R.; Shang, T.; Torrez, M.; Ronning, F.; Thompson, J.; Bauer, E. *J. Phys.: Condens. Matter* **2012**, *24*, 185702.
(48) Klünter, W.; Jung, W. *Z. Anorg. Allg. Chem.* **1995**, *621*, 197−200.
(49) Salamakha, P.; Gonçalves, A.; Sologub, O.; Almeida, M. *J. Alloys Compd.* **2003**, *360*, 61−68.
(50) Braunschweig, H.; Dewhurst, R. D.; Kraft, K.; Östreicher, S.; Radacki, K. *Angew. Chem., Int. Ed.* **2012**, *51*, 2183−2186.
(51) Leineweber, A.; Jacobs, H. *J. Alloys Compd.* **1998**, *278*, L10−L12.
(52) Schweitzer, K.; Jung, W. *Z. Anorg. Allg. Chem.* **1986**, *533*, 30−36.
(53) Braunschweig, H.; Radacki, K.; Scheschkewitz, D.; Whittell, G. R. *Angew. Chem., Int. Ed.* **2005**, *44*, 1658−1660.
(54) Braunschweig, H.; Radacki, K.; Rais, D.; Seeler, F. *Angew. Chem., Int. Ed.* **2006**, *45*, 1066−1069.
(55) Kurzman, J. A.; Moffitt, S. L.; Llobet, A.; Seshadri, R. *J. Solid State Chem.* **2011**, *184*, 1439−1444.
(56) Jensen, E. A.; Corbett, J. D. *Inorg. Chem.* **2002**, *41*, 6199−6205.
(57) Sologub, O.; Hiebl, K.; Salamakha, P. *Solid State Commun.* **2003**, *127*, 379−383.
(58) Janka, O.; Baumbach, R. E.; Thompson, J. D.; Bauer, E. D.; Kauzlarich, S. M. *J. Solid State Chem.* **2013**, *205*, 154−159.
(59) Schiffer, J.; Jung, W. *J. Solid State Chem.* **2000**, *154*, 232−237.
(60) Nagelschmitz, E.; Jung, W. *Chem. Mater.* **1998**, *10*, 3189−3195.
(61) (a) Hermus, M.; Geier, D.; Fokwa, B. P. *Z. Anorg. Allg. Chem.* **2012**, *638*, 49−52. (b) Hermus, M.; Fokwa, B. P. *Eur. J. Inorg. Chem.* **2014**, *2014*, 3085−3094.
(62) Hermus, M.; Scheifers, J. P.; Touzani, R.; Fokwa, B. P. *Inorg. Chem.* **2015**, *54*, 4056−4063.
(63) (a) Baumbach, R.; Chudo, H.; Yasuoka, H.; Ronning, F.; Bauer, E.; Thompson, J. *Phys. Rev. B: Condens. Matter Mater. Phys.* **2012**, *85*, 094422. (b) Matsuno, H.; Nohara, H.; Kotegawa, H.; Matsuoka, E.; Tomiyama, Y.; Sugawara, H.; Harima, H.; Tou, H. *J. Phys. Soc. Jpn.* **2012**, *81*, 073705.
(64) Matsuoka, E.; Tomiyama, Y.; Sugawara, H.; Sakurai, T.; Ohta, H. *J. Phys. Soc. Jpn.* **2012**, *81*, 043704.

DOI: 10.1021/acs.inorgchem.5b01275
Inorg. Chem. 2015, 54, 8049−8057